Parity nonconservation in the photodisintegration of the deuteron at low energy

C.-P. Liu,[1,2,*] C. H. Hyun,[3,4,†] and B. Desplanques[5,‡]
[1]*TRIUMF, 4004 Wesbrook Mall, Vancouver, British Columbia, Canada V6T 2A3*
[2]*Kernfysisch Versneller Instituut, Zernikelaan 25, Groningen 9747 AA, The Netherlands*
[3]*School of Physics, Seoul National University, Seoul, 151-742, Korea*
[4]*Institute of Basic Science, Sungkyunkwan University, Suwon 440-746, Korea*
[5]*Laboratoire de Physique Subatomique et de Cosmologie (UMR CNRS/IN2P3-UJF-INPG), F-38026 Grenoble Cedex, France*
(Received 2 March 2004; published 30 June 2004)

The parity-nonconserving asymmetry in the deuteron photodisintegration, $\vec{\gamma}+d\rightarrow n+p$, is considered with the photon energy ranged up to 10 MeV above the threshold. The aim is to improve upon a schematic estimate assuming the absence of tensor, as well as spin-orbit forces in the nucleon-nucleon interaction. The major contributions are due to the vector-meson exchanges, and the strong suppression of the pion-exchange contribution is confirmed. A simple argument, going beyond the observation of an algebraic cancellation, is presented. Contributions of meson-exchange currents are also considered, but found to be less significant.

DOI: 10.1103/PhysRevC.69.065502 PACS number(s): 24.80.+y, 25.20.Dc, 11.30.Er

I. INTRODUCTION

Some interest, both experimental and theoretical, has recently been shown for the study of parity nonconservation in the deuteron photodisintegration by polarized light. Historically, it was its inverse counterpart: the net polarization in radiative thermal neutron capture by proton, $n+p\rightarrow d+\gamma$, which attracted the first attention [1]. The experimental study was performed by the Leningrad group, taking advantage of new techniques measuring an integrated current [2]. The nonzero polarization obtained, $P_\gamma=-(1.3\pm0.45)\times10^{-6}$, motivated many theoretical calculations in the frame of strong and weak interaction models known in the 1970s (see, for instance, Refs. [3–5]. The theoretical results were consistently within the range $P_\gamma=(2-5)\times10^{-8}$, which is smaller than the measurement by a factor of 30 or more in magnitude and, moreover, of opposite sign. The difficulty in understanding the measurement and, also perhaps, the novelty of the techniques, which have been extensively used later on, led to a special reference to this work as the "Lobashov experiment."

Later estimates with modern nucleon-nucleon (NN) potentials, both parity-conserving (PC) and parity-nonconserving (PNC), give values of P_γ roughly within the same theoretical range as above. On the experimental side, new results were reported in the early 1980s by the same Leningrad group, giving $P_\gamma\leqslant5\times10^{-7}$ [6] and $P_\gamma=(1.8\pm1.8)\times10^{-7}$ [7]. Practically, these results indicate an upper limit of P_γ, which is not very constrictive. Since the Leningrad group's last report, the "Lobashov experiment" has long been forgotten by both experimentalists and theorists. Recent experiments, such as elastic $\vec{p}$-p scattering (TRIUMF [8]) and polarized thermal neutron capture by proton (LANSCE [9]), which directly address the problem of PNC NN interactions, and quasielastic $\vec{e}$-d scattering (MIT-Bates [10,11]), which indirectly involves these interactions, have however raised a new interest for the study of PNC effects in few-body systems. In what could be a golden age for these studies, the "Lobashov experiment" is again evoked.

While it seems that there is not much prospect for performing the "Lobashov experiment" in the near future, the inverse process, on the contrary, could be more promising. In this reaction, $\vec{\gamma}+d\rightarrow n+p$, where a deuteron is disintegrated by absorbing a circularly polarized photon, it is expected that, near threshold, the PNC asymmetry (A_γ) is equal to the polarization in the "Lobashov experiment." This last one can thus be tested from a different approach.

The asymmetry A_γ in the deuteron photodisintegration was first calculated by Lee [12] up to the photon energy $\omega_\gamma\simeq3.22$ MeV, which is 1 MeV above the threshold. In this energy domain, where the dominant regular transition is $M1$, the result was within the theoretical range of P_γ. Later on, Oka extended Lee's work, up to $\omega_\gamma\simeq35$ MeV [13]. Though the cross section still receives a contribution from the $M1$ transition, the dominant contribution comes from the $E1$ transitions. This offers a pattern of PNC effects different from the one at very low photon energy. It was found that A_γ shows a great enhancement at $\omega_\gamma\gtrsim5$ MeV, mainly due to the PNC π-exchange contribution. If such an enhancement was observed in the experiment, it would provide an important and unambiguous determination of the weak πNN coupling constant h^1_π. However, a recent schematic calculation of A_γ by Khriplovich and Korkin [14], partly suggested by one of the present authors, showed a critical contradiction to Oka's result, with a huge suppression of A_γ at the energies $\omega_\gamma\gtrsim3$ MeV.

On the experimental side, a measurement of the asymmetry A_γ in $\vec{\gamma}+d\rightarrow n+p$ was considered in the 1980s by Earle *et al.* [15,16], but no sensitive result was reported. However, due to advances in experimental techniques and instrumentation, the measurement of A_γ becomes more feasible nowadays and several groups at JLab [17], IASA (Athens), LEGS

*Electonic address: c.p.liu@kvi.nl
†Electronic address: hch@meson.skku.ac.kr
‡Electronic address: desplanq@lpsc.in2p3.fr

(BNL), TUNL, and SPring-8 show interest in such a measurement. It is therefore important to understand and improve previous estimates.

In this work, we carefully reexamine the $\vec{\gamma}+d\rightarrow n+p$ process with two main purposes:

(1) To determine how the enhancement of the h_π^1 contribution in Oka's results will change when the calculation is completed with missing parity-admixed components in the final state, in particular in the $^3P_1$ channel. The role of this last one was revealed by the schematic estimate of Ref. [14].

(2) To determine the uncertainty of Khriplovich and Korkin's calculation in which very simple wave functions are used.

It is straightforward to deal with point (1). In Ref. [14], a nice and simple argument about the cancellation of the h_π^1 contribution from the final $^3P_0$, $^3P_1$, and $^3P_2$ states along with their parity-admixed partners was given. However, the argument assumed the absence of tensor as well as spin-orbit forces, which are important components of the *NN* interaction. In order to address these two points (missing components and simplicity of the wave functions), we elaborate our calculation with the Argonne v_{18} *NN* interaction model. We thus include the $^1S_0$, $^3P_0$, $^3P_1$, $^3P_2$-$^3F_2$ channels, deuteron *D* state, and all their parity-admixed partners consistently. They represent a minimal set of states that allows one to verify the results of the schematic model, as well as to include the effect of the tensor and spin-orbit forces that manifest differently in these various channels. We also include other channels, whose role is less important however. As for the *E*1 operator, we employ the Siegert's theorem [18], which takes into account the contribution of some PC and PNC two-body currents. The small photon energy considered here ($\omega_\gamma \leqslant 12$ MeV) justifies this usage. Since there is no theorem similar to the Siegert one for the *M*1 transition operator, two-body currents have to be considered explicitly for both the PC and PNC parts. Adopting the Desplanques, Donoghue, Holstein (DDH) potential of the weak interaction [19], the asymmetry A_γ will be expressed in terms of the weak πNN, ρNN and ωNN coupling constants, with corresponding coefficients indicating their relative importance.

This paper is organized as follows. In Sec. II, we review the basic formalism underlying the calculation, which involves both one- and two-body currents. In Sec. III, we show the results and some discussions follow. Particular attention is given to a comparison with earlier works and to new contributions from PNC two-body currents. A simple argument explaining the suppression of the pion-exchange contribution is also given. Conclusions are given in Sec. IV. The Appendix contains expressions of *E*1 and *M*1 transition amplitudes due to the PNC two-body currents considered in the present work.

II. FORMALISM

For a photodisintegration of an unpolarized target, the asymmetry factor is defined as

$$A_\gamma \equiv \frac{\sigma_+ - \sigma_-}{\sigma_+ + \sigma_-},$$

where $\sigma_{+(-)}$ denotes the total cross section using right- (left-) handed polarized light. By spherical multipole expansion, it could be expressed as

$$A_\gamma = \frac{2\ \mathrm{Re}\sum_{f,i,J}[F_{EJ}^* \tilde{F}_{MJ_5} + F_{MJ}^* \tilde{F}_{EJ_5}]}{\sum_{f,i,J}[F_{EJ}^2 + F_{MJ}^2]}. \quad (1)$$

In this formula, the normal electromagnetic (EM) and PNC-induced EM form factors, F_{XJ} and $\tilde{F}_{XJ_5}$, with *X* and *J* denoting the type and multipolarity of the transition between a specific initial (i) and final (f) states, are defined in the same way as Refs. [20,21]. They depend on the momentum transfer q, which equals to the photon energy ω_γ in this current case. The form factors $\tilde{F}_{XJ_5}$ vanish (and so does the asymmetry) unless some PNC mechanism induces parity admixtures of wave functions and axial-vector currents.

In this work, we consider the photon energy $\omega_\gamma = q$ up to 10 MeV above the threshold. As the long wavelength limit $\langle q\ r\rangle \ll 1$ is a good approximation, the inclusion of only dipole transitions, i.e., *E*1 and *M*1, is sufficient. This leads to 10 possible exit channels connected to the deuteron state by angular momentum considerations. Among them, $^1S_0$, via the *M*1 transition, and $^3P_0$, $^3P_1$, $^3P_2$-$^3F_2$, via the *E*1 transitions, dominate the cross section.

The transverse multipole operators assume a full knowledge of nuclear currents. This requires, besides the one-body current $\mathbf{j}^{(1)}$ from individual nucleons, a complete set of two-body exchange currents (ECs) $\mathbf{j}^{(2)}$, which is consistent with the *NN* potential. These ECs are usually the sources of theoretical uncertainties, because the *NN* dynamics is still not fully understood. While there is no alternative for the evaluation of F_{MJ}, the Siegert theorem [18] does allow one to transform the evaluation of F_{EJ} into the one of charge multipole F_{CJ}. The fact that the PC *NN* interaction does not give rise to exchange charges at $O(1)$ removes most of the uncertainties related to exchange effects: knowledge of the one-body charge $\rho^{(1)}$ is sufficient for a calculation good to the order of $1/m_N$.

In the framework of impulse approximation and using the Siegert theorem, one gets, for the deuteron photodisintegration ($E_f - E_i = \omega_\gamma = q$ and $J_i = 1$),

$$F_{E1}^{(S)}(q)_{f,i} = \frac{E_i - E_f}{q}\sqrt{\frac{2}{2J_i+1}}\langle J_f \| \int d^3x [j_1(qx) Y_1(\Omega_x)] \rho^{(1)}(\mathbf{x}) \| J_i\rangle$$
$$+ \frac{1}{q}\frac{1}{\sqrt{2J_i+1}}\langle J_f \| \int d^3x\, \boldsymbol{\nabla} \times [j_1(qx)\mathbf{Y}_{111}(\Omega_x)] \cdot \mathbf{j}_{\mathrm{spin}}^{(1)}(\mathbf{x}) \| J_i\rangle \simeq -\frac{q}{3\sqrt{2\pi}}\langle J_f \| \sum_i \hat{e}_i \mathbf{x}_i \| J_i\rangle \equiv -\frac{q}{2\sqrt{6\pi}}\langle E1^{(1)}\rangle, \quad (2)$$

$$F^{(1)}_{M1}(q)_{f,i} = i\frac{1}{\sqrt{2J_i+1}}\langle J_f\|\int d^3x[j_1(qx)\mathbf{Y}_{111}(\Omega_x)]\cdot\mathbf{j}^{(1)}(\mathbf{x})\|J_i\rangle \simeq -\frac{q}{3\sqrt{2\pi}}\langle J_f\|\sum_i\frac{1}{2m_N}[\hat{e}_i\mathbf{x}_i\times\mathbf{p}_i+\hat{\mu}_i\boldsymbol{\sigma}_i]\|J_i\rangle \equiv -\frac{q}{2\sqrt{6\pi}}\langle M1^{(1)}\rangle, \tag{3}$$

where $\hat{e}_i = e(1+\tau_i^z)/2$ and $\hat{\mu}_i = e(\mu_s+\mu_v\tau_i^z)/2$ with $\mu_s = 0.88$ and $\mu_v = 4.70$; Y and $\mathbf{Y}$ are the spherical and vector spherical harmonics. In these expressions, the approximated results are obtained by replacing the spherical Bessel function $j_1(qx)$ with its asymptotic form as $q\to 0$, i.e., $qx/3$, at the long wavelength limit and keeping terms linear in q (the lowest order); they could be related to the forms of $\langle E1^{(1)}\rangle$ and $\langle M1^{(1)}\rangle$ often adopted in the literature. In our numerical calculation, the identity relations are employed instead. Note that the one-body spin current is conserved by itself and not constrained by current conservation. In Eq. (2), this one-body spin current (2nd line) is of higher order in q compared with the Siegert term (1st line), however, it is kept for completeness. As for the PNC-induced form factors $\tilde{F}^{(S)}_{E1_5}$ and $\tilde{F}^{(1)}_{M1_5}$, one only has to replace either the initial or final state by its opposite-parity admixture, $\langle\tilde{J}_f|$ or $|\tilde{J}_i\rangle$, and add a factor "i" for $E1$ or "$-i$" for $M1$ matrix elements (in relation with our conventions).

The nonvanishing matrix elements for the five dominant exit channels are thus

(1) $^1S_0$:

$$\langle M1^{(1)}\rangle = -\frac{\mu_v}{m_N}\int dr U^*(^1S_0)U_d(^3S_1), \tag{4}$$

$$\langle E1^{(1)}_5\rangle = \frac{i}{3}\int r\,dr\,\tilde{U}^*(^3P_0)[U_d(^3S_1)-\sqrt{2}U_d(^3D_1)] - \frac{i}{\sqrt{3}}\int r\,dr\,U^*(^1S_0)\tilde{U}_d(^1P_1). \tag{5}$$

(2) $^3P_0$:

$$\langle E1^{(1)}\rangle = \frac{1}{3}\int r\,dr\,U^*(^3P_0)[U_d(^3S_1)-\sqrt{2}U_d(^3D_1)], \tag{6}$$

$$\langle M1^{(1)}_5\rangle = i\frac{\mu_v}{m_N}\int dr\left[\tilde{U}^*(^1S_0)U_d(^3S_1)-\frac{1}{\sqrt{3}}U^*(^3P_0)\tilde{U}_d(^1P_1)\right] - i\sqrt{\frac{2}{3}}\frac{\mu_s-1/2}{m_N}\int dr\,U^*(^3P_0)\tilde{U}_d(^3P_1). \tag{7}$$

(3) $^3P_1$:

$$\langle E1^{(1)}\rangle = -\frac{1}{\sqrt{3}}\int r\,dr\,U^*(^3P_1)\left[U_d(^3S_1)+\frac{1}{\sqrt{2}}U_d(^3D_1)\right], \tag{8}$$

$$\langle M1^{(1)}_5\rangle = -i\frac{\mu_v}{m_N}\int dr\,U^*(^3P_1)\tilde{U}_d(^1P_1) - i\frac{\mu_s+1/2}{\sqrt{2}m_N}\int dr\,U^*(^3P_1)\tilde{U}_d(^3P_1) - i\frac{\sqrt{2}\mu_s}{m_N}\int dr\,\tilde{U}^*(^3S_1)U_d(^3S_1) + i\frac{\mu_s-3/2}{\sqrt{2}m_N}\int dr\,\tilde{U}^*(^3D_1)U_d(^3D_1). \tag{9}$$

(4) $^3P_2$-$^3F_2$:

$$\langle E1^{(1)}\rangle = \frac{\sqrt{5}}{3}\int r\,dr\left\{U^*(^3P_2)\left[U_d(^3S_1)-\frac{1}{5\sqrt{2}}U_d(^3D_1)\right]+\frac{3\sqrt{3}}{5}U^*(^3F_2)U_d(^3D_1)\right\}, \tag{10}$$

$$\langle M1_5^{(1)}\rangle = -i\sqrt{\frac{5}{3}}\frac{\mu_v}{m_N}\int dr\left[U^*(^3P_2)\tilde{U}_d(^1P_1) - \sqrt{\frac{3}{5}}\tilde{U}^*(^1D_2)U_d(^3D_1)\right] + i\sqrt{\frac{5}{6}}\frac{\mu_s - 1/2}{m_N}\int dr\left[U^*(^3P_2)\tilde{U}_d(^3P_1) + \frac{3}{\sqrt{5}}\tilde{U}^*(^3D_2)U_d(^3D_1)\right]. \quad (11)$$

The results for the remaining five less important channels ($^3S_1$–$^3D_1$, $^1P_1$, $^1D_2$, $^3D_2$) will be included in numerical works. The r-weighted radial wave functions for scattering and deuteron states, U and U_d, along with their parity admixtures, $\tilde{U}$ and $\tilde{U}_d$, are obtained by solving the Schrödinger equations. The details can be found in Ref. [21].

By taking the square of normal EM form factors (PC response function) or the product of normal and PNC-induced ones (PNC response function), we can directly compare Eqs. (5a)–(5h) in Ref. [13]. After removing factors due to wave-function normalizations, the differences are

(1) The parity admixture of the scattering $^3P_1$ state is included in our work: The admixtures $\tilde{U}(^3S_1)$ and $\tilde{U}(^3D_1)$ are solved from the inhomogeneous differential equations with the source term modulated by $U(^3P_1)$. They are not orthogonal to the deuteron state and thus should not be ignored. Actually, they are required to ensure the orthogonality of the deuteron and the $^3P_1$ scattering states once these are allowed to contain a parity-nonconserving component.

(2) The terms involving the scalar magnetic moment are different: Looking for instance at the $M1$ matrix element between $U(^3P_1)$ and $\tilde{U}_d(^3P_1)$, the effective $M1$ operator is proportional to $\mu_s\boldsymbol{S}+\boldsymbol{L}/2$. By the projection theorem, $\langle\boldsymbol{S}\rangle = \langle\boldsymbol{L}\rangle$, the overall factor should be $\mu_s+1/2$, not μ_s+1 as in Ref. [13].[1] It looks as if this work ignored the $1/2$ factor in front of the $\boldsymbol{L}$ operator.

Both points involve the spin-conserving PNC interaction, which is dominated by the pion exchange. Therefore, how these differences change the sensitivity of A_γ with respect to h_π^1 will be elaborated in the next section.

Now we discuss, in two steps, the extra contributions due to ECs when one tries to go beyond the impulse approximation together with the Siegert-theorem framework.

First, when PC ECs are included, their contribution to $M1$ matrix elements, $F_{M1}^{(2)}$, definitely needs to be calculated. On the other hand, as PC exchange charges are higher order in the nonrelativistic limit, $F_{E1}^{(S)}$ is supposed to take care of most two-body effects, and the remaining contribution $\Delta F_{E1}^{(2)}$ can be safely ignored. This argument also applies for the PNC-induced form factors involving the PC ECs: one needs to consider $\tilde{F}_{M1_5}^{(2)}$ but can leave out $\Delta\tilde{F}_{E1_5}^{(2)}$.

Second, the inclusion of PNC ECs, to the first order in weak interaction, only affects the PNC-induced form factors. The contribution $\tilde{F}_{M1_5}^{(2')}$ is calculated by using the $M1$ operator constructed from the PNC ECs and unperturbed wave functions (so we use a prime to remind us of the difference from parity-admixture contributions). One special feature of PNC ECs is that they do have exchange charges of $O(1)$ [22]. Therefore, one should include them in $\tilde{F}_{E1_5}^{(S')}$.

As a last remark, we note one advantage of nuclear PNC experiments in processes like photodisintegration or radiative capture. The real photon is "blind" to the nucleon anapole moment, which could contribute otherwise to PNC observables in virtual photon processes. Because this P-odd T-even nucleon moment is still poorly constrained both theoretically and experimentally, the interpretation of real-photon processes, like the one considered here, is thus comparatively easier.

III. RESULTS AND DISCUSSIONS

For practical purposes, we use the Argonne v_{18} [23] ($\mathrm{A}v_{18}$) and DDH [19] potentials as the PC and PNC NN interactions, respectively. In comparison with earlier works in the 1970s or the 1980s, a strong interaction model like $\mathrm{A}v_{18}$ offers the advantage that the singlet-scattering length is correctly reproduced, due to its charge dependence. Correcting results in this respect is therefore unnecessary.

The total cross section is plotted in Fig. 1 as a function of the photon energy and labeled as "IA+Sieg." Its separate contributions from $E1$ and $M1$ transitions are also shown on the same plot (labeled accordingly). The $M1$ transition only dominates near the threshold region; as the photon energy reaches about 1 MeV above the threshold, the $E1$ transition overwhelms. Away from the threshold, the calculated results agree well with both experiment and existing potential-model calculations up to 10 MeV [24]. Such a good agreement shows the usefulness of the Siegert theorem, by which most of the two-body effects are included. Compared with the curve labeled as "IA," the result of impulse approximation, one sees the increasing importance of these two-body contributions as ω_γ gets larger. On the contrary, because $M1$ matrix elements are purely one-body, we expect our near-threshold results smaller than experiment by about 10% [24]. This discrepancy, originally found in the radiative capture of thermal neutron by proton (the inverse of deuteron photodisintegration), requires various physics such as exchange currents and isobar configurations, to be fully explained. Here, we qualitatively estimate a 5% error for the calculation of F_{M1} near threshold.

When calculating the PNC-induced matrix elements with the DDH potential, we use the strong meson-nucleon coupling constants: $g_{\pi NN}=13.45$, $g_{\rho NN}=2.79$, and $g_{\omega NN}=8.37$;

[1] We also note that unlike our notation $\mu_{s,v}$ is used to denote the anomalous magnetic moments in Ref. [13].

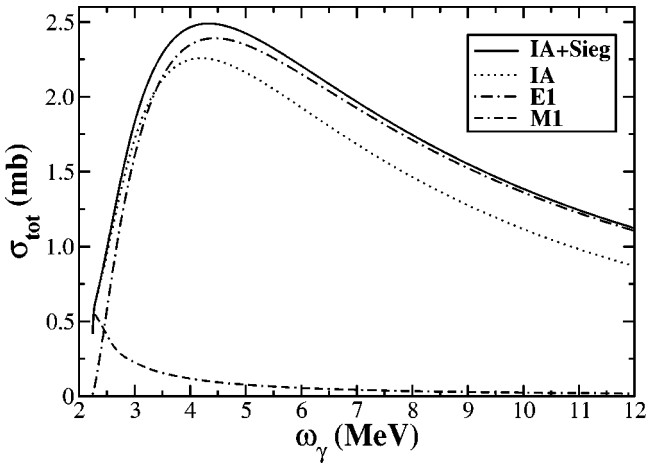

FIG. 1. The total cross section as a function of the photon energy. The main result is the curve labeled as "IA+Sieg," and the curves "E1" and "M1" showing contributions from corresponding transitions. The curve "IA" is the result of a pure impulse approximation calculation, where no two-body contribution is included.

and meson masses (in units of MeV): $m_\pi = 139.57$, $m_\rho = 770.00$, and $m_\omega = 781.94$. The resulting asymmetry is then expressed in terms of six PNC meson-nucleon coupling constants h's as

$$A_\gamma = c_1 h_\pi^1 + c_2 h_\rho^0 + c_3 h_\rho^1 + c_4 h_\rho^2 + c_5 h_\omega^0 + c_6 h_\omega^1, \qquad (12)$$

where the six energy-dependent coefficients $c_{1\ldots6}$ show the sensitivity to each corresponding coupling. It turns out that, for the energy range considered here, $c_2, c_4, c_5 \gg c_1 \gg c_3, c_6$. This implies that the asymmetry has a larger sensitivity to the isoscalar and isotensor couplings than to the isovector ones. The detailed energy dependences of these "large" and "small" coefficients are shown in Fig. 2.

In principle, these results are independent. In practice however, they can be shown to depend on three quantities, reflecting the dominant role of the various $S \leftrightarrow P$ neutron-proton transition amplitudes at low energy. These amplitudes have some energy dependence, which is essentially determined by the best known long-range properties of strong interaction models. They can therefore be parametrized by their values at zero energy [1,25,26], including at the deuteron pole. To a large extent, they can be used independently of the underlying strong interaction model, quite in the spirit of effective-field theories that they anticipated [27]. In the case of the Av_{18} model employed here, they are given by

$$m_N \lambda_t = -0.043 h_\rho^0 - 0.022 h_\omega^0,$$

$$m_N \lambda_s = -0.125 h_\rho^0 - 0.109 h_\omega^0 + 0.102 h_\rho^2,$$

$$m_N C = 1.023 h_\pi^1 + 0.007 h_\rho^1 - 0.021 h_\omega^1. \qquad (13)$$

The largest corrections to the above approach occur for the PNC pion-exchange interaction which, due to its long range, produces some extra energy dependence and sizable $P \leftrightarrow D$ transition amplitudes. They can show up when the contribution of the $S \leftrightarrow P$ transition amplitude is suppressed, as it is in this work.

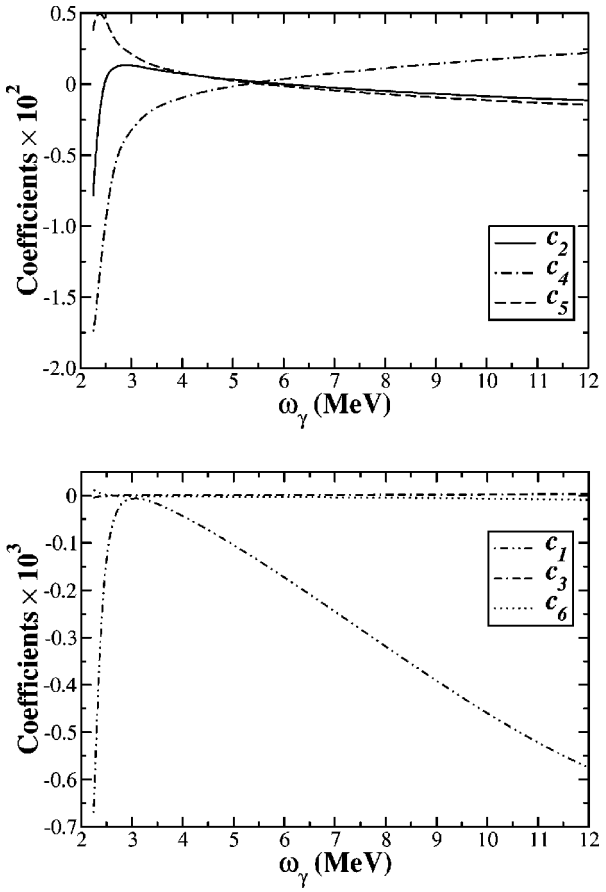

FIG. 2. The energy dependences of "large" coefficients c_2, c_4, and c_5 (top panel) and "small" coefficients c_1, c_3, and c_6 (bottom panel) in the asymmetry parametrization, Eq. (12).

For $\omega_\gamma = 2.235$ MeV, which is very close to the disintegration threshold, we get the asymmetry

$$A_\gamma^{(th)} \approx [-8.44 h_\rho^0 - 17.65 h_\rho^2 + 3.63 h_\omega^0 + O(c_1, c_3, c_6)] \times 10^{-3}. \qquad (14)$$

Using the DDH "best" values as an estimate, we obtained $A_\gamma^{(th)} \approx 2.53 \times 10^{-8}$. By detailed balancing, one expects that $A_\gamma^{(th)}$ equals the circular polarization $P_\gamma^{(th)}$ observed in the radiative thermal neutron capture by proton, given the same kinematics. Though our result does not exactly correspond to the same kinematics as the inverse process usually considered (the kinetic energy of thermal neutrons $\sim$0.025 eV), it agrees both in sign and order of magnitude with existing calculations of $P_\gamma^{(th)}$ [3–5]. We also performed a similar calculation for the latter case with Av_{18}, and the result is

$$P_\gamma^{(th)} \approx [-8.75 h_\rho^0 - 17.47 h_\rho^2 + 3.39 h_\omega^0 + O(c_1, c_3, c_6)] \times 10^{-3}. \qquad (15)$$

This is very close to the result of A_γ quoted above.

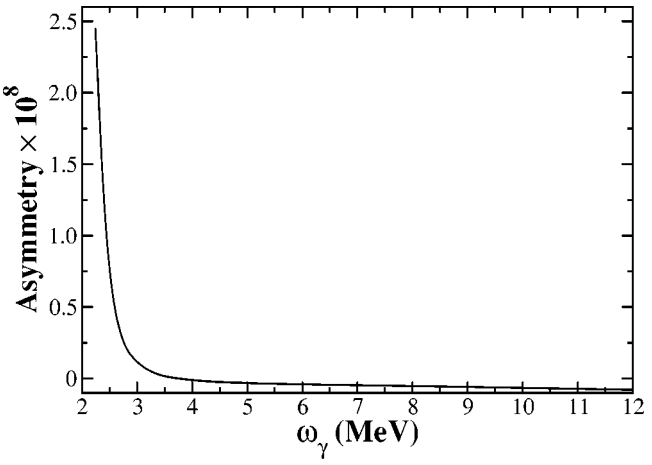

FIG. 3. The asymmetry by using the DDH best values.

It is noticed that our expression of $A_\gamma^{(th)}$ at very low energy, and therefore that one for $P_\gamma^{(th)}$, contains a contribution from the one-pion exchange (see the low-energy part of the c_1 coefficient given in Fig. 2). This feature, which apparently contradicts the statement often made in the past that this contribution is absent in $P_\gamma^{(th)}$, is due to the incorporation in our work of the spin term in Eq. (2), which represents a higher-order term in q. This correction also explains the difference in the behavior of the c_1 coefficient with Oka's result [13].

We note that, because the $M1$ transition dominates at the threshold and we only use the impulse approximation for its matrix element, there should be approximately a −5% correction to $A_\gamma^{(th)}$ (also $P_\gamma^{(th)}$) when two-body effects are included in F_{M1}. On the other hand, as $\widetilde{F}_{E1_5}$ is calculated using the Siegert theorem, it should be reliable up to the correction of $\widetilde{F}_{E1_5}^{(S')}$ from the PNC exchange charge at $O(1)$.

When the photon energy gets larger, one can see immediately that the asymmetry gets smaller. A prediction using the DDH best values is shown in Fig. 3. In this figure, as soon as the photon energy reaches 1 MeV above the threshold, the asymmetry drops by one order of magnitude. Moreover, the sign changes around ω_γ=4 MeV. This implies that a higher sensitivity ($\sim 10^{-9}$) is needed for any experiment targeting at the kinematic range away from the threshold. Our calculation is consistent with the work by Khriplovich and Korkin [14], but is widely different from the one by Oka [13]. In the following, we make a closer comparison with these works and, then, present the results for the contribution of various PNC two-body currents considered.

A. Comparison with Oka's work

The major difference comes from the pion sector. In Ref. [14], where the scattering wave functions are obtained from the zero-range approximation and the deuteron is purely a $^3S_1$ state, a simple angular momentum consideration leads to a null contribution from pions. Our result shows that the more complex nuclear dynamics has only small corrections, so the asymmetry is not sensitive to h_π^1. However, it is not the case at all in Ref. [13]: the pion exchange dominates the asymmetry with the coefficient c_1 being one or two orders of magnitude larger than our result.

TABLE I. The dominant PNC responses due to the pion exchange for ω_γ 10 MeV above the threshold (in units of $10^{-5}\times h_\pi^1$). The central column is calculated by Eqs. (4)–(11), while the right column by Eqs. (5a)–(5h) in Ref. [13]. The symbol $\mathcal{D}$ denotes the deuteron state.

Transitions	Equations (4)–(11)	Equations (5a)–(5h) in Ref. [13]
$^3P_0 \leftrightarrow \mathcal{D}$	0.449	−0.142
$^3P_1 \leftrightarrow \widetilde{\mathcal{D}}$	−3.217	−4.383
$\widetilde{^3P_1} \leftrightarrow \mathcal{D}$	3.942	Not considered
$^3P_2 \leftrightarrow \widetilde{\mathcal{D}}$	−1.231	0.389
$\widetilde{^3P_2} \leftrightarrow \mathcal{D}$	−0.142	0.045
$^3F_2 \leftrightarrow \widetilde{\mathcal{D}}$	−0.151	0.048
$\widetilde{^3F_2} \leftrightarrow \mathcal{D}$	−0.019	0.006
Total	−0.371	−4.037

This discrepancy could be illustrated by considering a case where ω_γ is 10 MeV above the threshold. In the central column of Table I, we list the pertinent PNC responses due to the pion exchange among the five dominant exit channels. In the right column, we simulate what the outcome will be if the analytical results of Eqs. (5a)–(5g) in Ref. [13] are used, i.e., with different factors involving μ_s and no parity admixture of the $^3P_1$ state as mentioned in Sec. II. Comparing the totals from both columns, one immediately observes that the simulated result is bigger by an order of magnitude. More inspection shows that, while the changes of the μ_s factors do alter each response somewhat, the major difference depends on whether the big cancellation from the $^3P_1$ admixture is included or not. By adding contributions from other subleading channels, the total will be further downed by a factor of 2.5. Thus the overall difference is about a factor of 30.

B. Comparison with Khriplovich and Korkin's work

The vanishing of the π-exchange contribution in Khriplovich and Korkin's work [14] supposes that the $E1$ transitions from the deuteron state to the different scattering states, $^3P_0$, $^3P_1$, and $^3P_2$, are the same, which implies that one neglects both the tensor and spin-orbit components of the strong interaction. As these parts of the force have large effects in some cases, it is important to determine how the above vanishing is affected when a more realistic description of the interaction is used.

We first notice that the isoscalar magnetic operator, $\mu_s \boldsymbol{S} + \boldsymbol{L}/2$, can be written as $\mu_s \boldsymbol{J} + (1/2 - \mu_s)\boldsymbol{L}$. As the operator $\boldsymbol{J}$ conserves the total angular momentum, it follows that the $E1$ transitions from the deuteron state to the $^3P_0$ and $^3P_2$ states will be proportional to $\mu_s - 1/2$, in agreement with Eqs. (7) and (11). A similar result holds for the $^3P_1$ state. For this transition, one has to take into account that the $\boldsymbol{J}$ operator connects states that are orthogonal to each other, including

the case where they contain some parity admixture. This unusual but interesting result was originally suggested by a similar result obtained by Khriplovich and Korkin for the $^1S_0$ and $^3P_0$ states [14]. They used it later on for the π-exchange contribution upon the suggestion of one the present authors. Taking this property into account, one can check that the different μ_s-dependent terms in Eq. (9) combine so that the quantity, $\mu_s - 1/2$, can be factored out. This explains the cancellation of the two largest contributions in Table I, 3.942 and −3.217, approximately proportional to $2\mu_s = 1.76$ and $-(\mu_s + 1/2) = -1.38$.

Further cancellation is obtained when one considers the sum of the π-exchange contributions to the asymmetry A_γ corresponding to the different P states. Taking into account the remark made in the previous paragraph, it can be checked that contributions from Eqs. (7), (9), and (11) are proportional to 2, 3, and −5 and 4, −3, and −1 for the $^3S_1$ and $^3D_1$ deuteron components, respectively (assuming that the ^3P wave functions are the same). As can be seen in Table I, the dominant contributions, $0.449, 0.725 (= 3.942 - 3.217)$, and −1.231 are not far from the relative ratios 2, 3, and −5, expected for the $^3S_1$ deuteron component. Possible departures can be ascribed in the first place to the $^3D_1$ deuteron component.

The above cancellation calls for an explanation deeper than the one consisting of the verification that the algebraic sum of different contributions cancels. An argument could be the following: In the conditions where the cancellation takes place (the same interaction in the ^3P states in particular), a closure approximation involving spin and angular orbital momentum degrees of freedom can be used to simplify the writing of the PNC part of the response function that appears at the numerator of Eq. (1). Keeping only the factors of interest here, the interference term of $E1$ and $M1$ matrix elements can be successively transformed as follows:

$$\begin{aligned}\delta R &\propto \sum_M \langle J_i | \hat{r}^i \left(\mu_s - \frac{1}{2} \right) L^j (\delta^{ij} - \hat{q}^i \hat{q}^j) | \widetilde{J_i} \rangle \\ &\propto \sum_M \left[\langle {}^3S_1 | U_d({}^3S_1) + \frac{U_d({}^3D_1)}{\sqrt{2}} (3(\boldsymbol{S}\cdot\hat{r})^2 - S^2) \right] \\ &\quad \times \hat{r}^i L^j (\delta^{ij} - \hat{q}^i \hat{q}^j) [\boldsymbol{S}\cdot\hat{r} | {}^3S_1 \rangle] \\ &\propto \mathrm{Tr} \left[\left(U_d({}^3S_1) + \frac{U_d({}^3D_1)}{\sqrt{2}} (3(\boldsymbol{S}\cdot\hat{r})^2 - S^2) \right) \boldsymbol{S}\cdot\hat{r} \right] = 0. \end{aligned} \tag{16}$$

The first line stems from retaining the isoscalar part of the magnetic operator proportional to $(\mu_s - 1/2)\boldsymbol{L}$ (it is reminded that the $\boldsymbol{J}$ part does not contribute). The next line is obtained by expressing the PC and PNC parts of the deuteron wave function as some operator acting on a pure $|{}^3S_1\rangle$ state. Once this transformation is made, it is possible to replace the summation over the deuteron angular momentum components, M, by the spin ones, m_s, which is accounted for at the third line. The last line then follows from the fact that the trace of the spin operator, $\boldsymbol{S}$, possibly combined with a $\Delta S = 2$ one, vanishes. A result similar to the above one can be obtained for some contributions involving MECs. It is however noticed that some corrections involving the spin-orbit force, or spin-dependent terms in the $E1$ transition operator, which both contain an extra $\boldsymbol{S}$ factor in the above equation, could lead to a nonzero trace and therefore to a relatively large correction. Of course, the above cancellation relies on the fact that no polarization of the initial or final state is considered. Had we looked at an observable involving such a polarization, like the asymmetry in the capture of polarized thermal neutrons by protons, the result will be quite different. As is well known, this observable is dominated by the π-exchange contribution [1].

C. Contributions of PNC ECs

In Sec. II, the contributions of PNC ECs were summarized in two additional PNC-induced form factors, $\widetilde{F}^{(S')}_{E1_5}$ and $\widetilde{F}^{(2')}_{M1_5}$. Now, we estimate these contributions by considering only the dominant channels $^1S_0$, $^3P_0$, $^3P_1$, and $^3P_2$-$^3F_2$. As $E1_5$ connects states of the same parity, only $^1S_0$ is allowed; therefore, $\widetilde{F}^{(S')}_{E1_5}$ plays a more important role for A_γ near the threshold. On the other hand, $M1_5$ connects states of opposite parity, which requires the other four channels, so $\widetilde{F}^{(2')}_{M1_5}$ has more impact on A_γ at higher energies. The full set of PNC ECs which is consistent with the DDH potential was derived in Ref. [22], Eqs. (17)–(24). The whole evaluation is straightforward, however tedious, so we defer all the analytical expressions in the Appendix and only quote the numerical results here.

With the same parametrization as Eq. (12), the additional contributions to the asymmetry by PNC ECs, via $E1_5$ and $M1_5$ respectively, are

$$A_\gamma(\widetilde{F}^{(S')}_{E1_5}) = c_2^{(S')} h_\rho^0 + c_4^{(S')} h_\rho^2, \tag{17}$$

$$A_\gamma(\widetilde{F}^{(2')}_{M1_5}) = c_1^{(2')} h_\pi^1 + c_2^{(2')} h_\rho^0 + c_3^{(2')} h_\rho^1 + c_4^{(2')} h_\rho^2 + c_6^{(2')} h_\omega^1. \tag{18}$$

The detailed energy dependence of each coefficient is shown in Fig. 4.

The dominance of $\widetilde{F}^{(S')}_{E1_5}$ near the threshold and $\widetilde{F}^{(2')}_{M1_5}$ at higher energies could be readily observed in these plots. We discuss their significances to the total asymmetry in the following.

For the case where the photon energy is 0.01 MeV above the threshold, only $c_2^{(S')}$ and $c_4^{(S')}$ are substantial. The former coefficient is about 20% of c_2, while the latter one is only 2% of c_4. By using the DDH best values, these contributions give an asymmetry of about 1.4×10^{-9}, which is a 6% correction. This is typically the order of magnitude one could expect from the exchange effects.

As the energy gets larger, while the coefficients $c_2^{(S')}$ and $c_4^{(S')}$ keep stable, the coefficients associated with $M1_5$ matrix elements grow linearly, roughly. The fastest growing one is $c_1^{(2')}$, because the long-ranged pion exchange dominates the

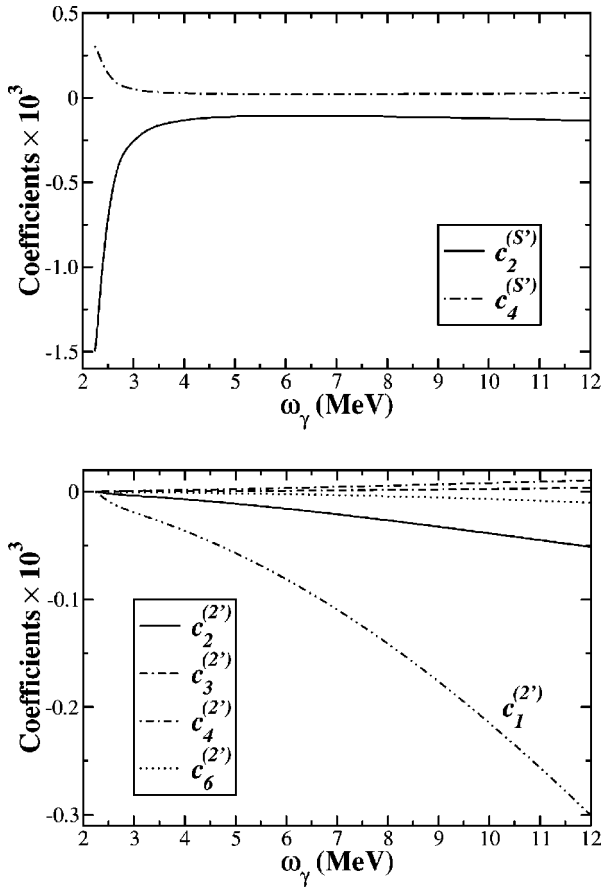

FIG. 4. The energy dependences of PNC EC coefficients in the asymmetry parametrization: the top panel shows $c_{2,4}^{(S')}$ in Eq. (17) and the bottom panel shows $c_{1,2,3,4,6}^{(2')}$ of Eq. (18).

matrix elements. Comparatively, $c_2^{(2')}$ has a smaller slope due to less overlap between the effective ranges pertinent to the deuteron wave function and the ρ exchange.

For the case where the photon energy is 10 MeV above the threshold, $c_1^{(2')}$, $c_2^{(2')}$, and $c_2^{(S')}$ are substantial. The first coefficient is about 50% of c_1, and the latter two combined is about 16% of c_2. The extremely large correction to c_1 can be simply explained. The cancellation which affects the single-particle contribution [see Eq. (16)] does not apply to the two-body one. By using the DDH best values, all contributions due to PNC ECs give an asymmetry of about 3.7×10^{-11}, which is a 5% correction. The reason why large effects from individual meson exchanges lead to an overall small correction is due to the cancellation between pion and heavy-meson exchanges: the DDH best values have opposite signs for the pion and heavy-meson couplings. This conclusion, however, depends on the sign we assumed for the $g_{\rho\pi\gamma}$ coupling.

IV. CONCLUSION

The present work has been motivated by various aspects of the PNC asymmetry A_γ in the deuteron photodisintegration, especially in the few-MeV photon-energy range. An earlier work addressing this energy domain [13] showed that the process could provide information on the PNC πNN coupling constant, h_π^1, which allows one to check results from other processes involving this coupling. A later work [14], rather schematic, concluded that this contribution could be largely suppressed. Between these two extreme limits, the question arises of what this contribution could be when a realistic description is made, including in particular the tensor and spin-orbit components of the *NN* interaction. At first sight, a sizable PNC π-exchange contribution could arise if one assumes tensor-force effects of about 15% for each partial contribution and no cancellation.

The complete calculation shows that the π-exchange contribution remains strongly suppressed after improving upon the schematic model. Beyond making this observation, a genuine explanation should therefore be found. When considering the asymmetry A_γ, an average is made over the spins of initial and final states. Terms in the interference effects of electric and magnetic transitions, whose spin dependence averages to a nonzero value, are expected to produce a sizable contribution. This discards the π-exchange contribution, which involves a linear dependence on the spin operator $\boldsymbol{S}$, and tensor-force effects, which involve the product of spin operators of the orders 1 and 2. The argument applies to MECs too. A different conclusion would hold for an observable implying a spin polarization of the initial or final state. It thus appears some similarity between the relative role of various contributions here and that one emphasized by Danilov for the inverse process at thermal energies: the circular polarization of photons P_γ (equivalent to A_γ here) is mainly dependent on the PNC isoscalar and isotensor contributions, while the asymmetry of the photon emission with respect to the neutron polarization depends on the π-exchange contribution.

As the π-exchange contribution to the asymmetry A_γ turns out to have a minor role, we can concentrate on the vector-meson ones. At the low energies considered here, it is expected that these contributions depend on two combinations of parameters entering the description of the PNC (and PC) *NN* interaction. They are the zero-energy neutron-proton scattering amplitudes in the $T=0$ and $T=1$ channels, λ_t and λ_s. In terms of these quantities introduced by Danilov [1] (see also later works by Missimer [25], Desplanques and Missimer [26], and Holstein [27]), the discussion could be simpler. The asymmetry is found to vary between

$$A_\gamma = 0.70 m_N \lambda_t - 0.17 m_N \lambda_s \text{ at threshold}$$

and

$$A_\gamma = -0.037 m_N \lambda_t + 0.022 m_N \lambda_s \quad \text{at} \quad \omega_\gamma = 12 \text{ MeV},$$

thus evidencing a change in sign which occurs around $\omega_\gamma = 5.5$ MeV for both amplitudes. Depending on low-energy properties and, thus, on the best-known properties of the strong interaction, the place where the cancellation of A_γ occurs sounds to be well established. It roughly agrees with what can be inferred from the analytic work by Khriplovich and Korkin [14]. Not much sensitivity to PNC ECs is found. An experiment should therefore aim at a measurement at

energies significantly different, either below or above.

The goal for studying PNC effects is to get information on the hadronic physics entering the PNC *NN* interaction. This supposes that one can disentangle the different contributions to each process. We notice that the combination of parameters λ_t and λ_s appearing in the expression of A_γ is orthogonal to that one determining PNC effects in most other processes, especially in medium and heavy nuclei. The study of the present process is therefore quite useful. Another observation, which is not totally independent of the previous one, concerns the isotensor contribution. This one is especially favored in the present process, while it is generally suppressed in processes involving a roughly equal number of protons and neutrons with either spin [28]. The present process is therefore among the best ones to get information on the isotensor ρNN coupling constant. We, however, stress that this supposes the isoscalar parts could be constrained well by other processes. In a meson-exchange model of the PNC interaction, these are represented by the isoscalar ρNN and ωNN coupling constants. One could add that the relative sign of these two contributions is the same, in a large range of the photon energy ($\omega_\gamma \geqslant 3$ MeV), as in many other processes. It however differs at small photon energies, where the asymmetry involves a combination of the various isoscalar and isotensor couplings that is little constrained by other processes. This explains that expectations of A_γ up to 10^{-7} near threshold could be suggested in recent works on the basis of a phenomenological analysis [14,28,29]. Measuring this asymmetry could therefore be quite useful to determine a poorly known component of PNC *NN* interactions. On the theoretical side, the present work should be completed by the contribution of further parity-conserving exchange currents, but also by higher $1/m_N$-order corrections from the single-particle current and, consistently, from both PC and PNC exchange currents [30]. Though they are not expected to change the main conclusions reached here, they could be required to obtain from experiments more accurate information on PNC *NN* forces.

ACKNOWLEDGMENTS

C.-P. L. would like to thank R. Schiavilla, M. Fujiwara, and A. I. Titov for useful disussions. C.H.H. gratefully acknowledges the hospitality of the Laboratoire de Physique Subatomique et de Cosmologie, where part of this work was performed. The work of C.H.H. is partially supported by Korea Research Foundation (Grant No. KRF-2003-070-C00015).

APPENDIX: NONVANISHING MATRIX ELEMENTS OF PNC ECS FOR DOMINANT TRANSITIONS

In this section, we summarize the analytical expressions of the nonzero $\widetilde{F}^{(S')}_{E1_5}$ and $\widetilde{F}^{(2')}_{M1_5}$ for the five dominant channels which lead to the numerical results in Sec. III C.

1. $\widetilde{F}^{(S')}_{E1_5}$

As discussed in Sec. II, an exchange charge at $O(1)$ should contribute to this form factor. According to Ref. [22], the ρ exchange does generate one:

$$\rho^{\rho}_{mesonic}(\boldsymbol{x};\boldsymbol{r}_1,\boldsymbol{r}_2) = 2eg_{\rho NN}\left(h^0_\rho - \frac{h^2_\rho}{2\sqrt{6}}\right)(\boldsymbol{\tau}_1\times\boldsymbol{\tau}_2)^z(\boldsymbol{\sigma}_1-\boldsymbol{\sigma}_2)\cdot\boldsymbol{\nabla}_x[f_\rho(r_{x1})f_\rho(r_{x2})], \tag{A1}$$

with $f_X(r)=\exp(-m_X r)/(4\pi r)$ and $r_{xi}=|\boldsymbol{x}-\boldsymbol{r}_i|$. The $^1S_0$ state is the only open exit channel and it gives

$$\langle E1^{(S')}_5\rangle = 8\frac{g_{\rho NN}}{m_\rho}\left(h^0_\rho - \frac{h^2_\rho}{2\sqrt{6}}\right)\langle {}^1S_0|rf_\rho(r)|{}^3S_1\rangle_d, \tag{A2}$$

where $\langle f|F(r)|i\rangle_d$ denotes the radial integral $\int dr U^*(f)F(r)U_d(i)$ and the subscript "*d*" refers to the deuteron state.

2. $\widetilde{F}^{(2')}_{M1_5}$

As the four allowed exit channels $^3P_0$, $^3P_1$, and $^3P_2-{}^3F_2$ are spin- and isospin- triplet, the nonvanishing PNC ECs, which satisfy the spin and isospin selection rules, are

$$\boldsymbol{j}^{\rho}_{pair}(\boldsymbol{x};\boldsymbol{r}_1,\boldsymbol{r}_2) = \frac{eg_{\rho NN}}{4m_N}h^1_\rho f_\rho(r)(\tau^z_1-\tau^z_2)(\boldsymbol{\sigma}_1+\boldsymbol{\sigma}_2)[(1+\tau^z_1)\delta^{(3)}(\boldsymbol{x}-\boldsymbol{r}_1)] + (1\leftrightarrow 2), \tag{A3}$$

$$\boldsymbol{j}^{\omega}_{pair}(\boldsymbol{x};\boldsymbol{r}_1,\boldsymbol{r}_2) = \frac{-eg_{\omega NN}}{4m_N}h^1_\omega f_\omega(r)(\tau^z_1-\tau^z_2)(\boldsymbol{\sigma}_1+\boldsymbol{\sigma}_2)[(1+\tau^z_1)\delta^{(3)}(\boldsymbol{x}-\boldsymbol{r}_1)] + (1\leftrightarrow 2), \tag{A4}$$

$$\boldsymbol{j}^{\rho}_{mesonic}(\boldsymbol{x};\boldsymbol{r}_1,\boldsymbol{r}_2) = \frac{-eg_{\rho NN}}{m_N}\left(h^0_\rho - \frac{h^2_\rho}{2\sqrt{6}}\right)(\boldsymbol{\tau}_1\times\boldsymbol{\tau}_2)^z\nabla^a_x\{i[\nabla^a_1\boldsymbol{\sigma}_2+\sigma^a_1\boldsymbol{\nabla}_2, f_\rho(r_{x1})f_\rho(r_{x2})] - \mu_v[(\boldsymbol{\sigma}_1\times\boldsymbol{\nabla}_1)^a\boldsymbol{\sigma}_2+\sigma^a_1\boldsymbol{\sigma}_2 \times\boldsymbol{\nabla}_2, f_\rho(r_{x1})f_\rho(r_{x2})]\} + (1\leftrightarrow 2), \tag{A5}$$

$$\boldsymbol{j}^{\rho\pi}_{mesonic}(\boldsymbol{x};\boldsymbol{r}_1,\boldsymbol{r}_2) = \frac{-eg_{\rho NN}g_{\rho\pi\gamma}}{\sqrt{2}m_\rho}h^1_\pi(\boldsymbol{\tau}_1\times\boldsymbol{\tau}_2)^z(\boldsymbol{\nabla}_1\times\boldsymbol{\nabla}_2)[f_\rho(r_{x1})f_\pi(r_{x2})] + (1\leftrightarrow 2). \tag{A6}$$

Note that one additional strong meson-nucleon coupling constant, $g_{\rho\pi\gamma}$, appears in Eq. (A6). This could be constrained by the $\rho\rightarrow\pi+\gamma$ data. For the numerical calculation, we quote the number $g_{\rho\pi\gamma}=0.585$ as given in Ref. [31]. The matrix element $\langle M1^{(2')}_5\rangle$ can be written as a sum of the contributions from each EC as

$$\langle M1^{(2')}_5\rangle = \frac{1}{m_N}\left[g_{\rho NN}h^1_\rho X_1 + g_{\omega NN}h^1_\omega X_2 + g_{\rho NN}\left(h^0_\rho - \frac{h^2_\rho}{2\sqrt{6}}\right)X_3\right] + \frac{1}{m_\rho}g_{\rho NN}g_{\rho\pi\gamma}h^1_\pi X_4, \tag{A7}$$

and for each exit channel, the quantities X_{1-4} are

(1) $^3P_0$

$$X_1 = -\frac{2}{3}\left(\langle {}^3P_0|rf_\rho(r)|{}^3S_1\rangle_d + \frac{1}{\sqrt{2}}\langle {}^3P_0|rf_\rho(r)|{}^3D_1\rangle_d\right), \tag{A8}$$

$$X_2 = \frac{2}{3}\left(\langle {}^3P_0|rf_\omega(r)|{}^3S_1\rangle_d + \frac{1}{\sqrt{2}}\langle {}^3P_0|rf_\omega(r)|{}^3D_1\rangle_d\right), \tag{A9}$$

$$\begin{aligned} X_3 = -\frac{8}{3}\Bigg[&(1+2\mu_v)\langle {}^3P_0|rf_\rho(r)|{}^3S_1\rangle_d \\ &+ \frac{1}{\sqrt{2}}(1-\mu_v)\langle {}^3P_0|rf_\rho(r)|{}^3D_1\rangle_d - \frac{2}{m_\rho}\langle {}^3P_0|rf_\rho(r)|{}^3S^{(+)}_1\rangle_d \\ &- \frac{\sqrt{2}}{m_\rho}\langle {}^3P_0|rf_\rho(r)|{}^3D^{(-)}_1\rangle_d\Bigg], \end{aligned} \tag{A10}$$

$$X_4 = \frac{4\sqrt{2}}{3(m^2_\rho - m^2_\pi)}[\langle {}^3P_0|f'_{\pi\rho}(r)|{}^3S_1\rangle_d - \sqrt{2}\langle {}^3P_0|f'_{\pi\rho}(r)|{}^3D_1\rangle_d]; \tag{A11}$$

(2) $^3P_1$

$$X_1 = \frac{1}{\sqrt{3}}[\langle {}^3P_1|rf_\rho(r)|{}^3S_1\rangle_d - \sqrt{2}\langle {}^3P_1|rf_\rho(r)|{}^3D_1\rangle_d], \tag{A12}$$

$$X_2 = -\frac{1}{\sqrt{3}}[\langle {}^3P_1|rf_\omega(r)|{}^3S_1\rangle_d - \sqrt{2}\langle {}^3P_1|rf_\omega(r)|{}^3D_1\rangle_d], \tag{A13}$$

$$\begin{aligned} X_3 = \frac{4}{\sqrt{3}}\Bigg[&(1-\mu_v)\langle {}^3P_1|rf_\rho(r)|{}^3S_1\rangle_d \\ &- \sqrt{2}(1-\mu_v)\langle {}^3P_1|rf_\rho(r)|{}^3D_1\rangle_d - \frac{2}{m_\rho}\langle {}^3P_1|rf_\rho(r)|{}^3S^{(+)}_1\rangle_d \\ &+ \frac{2\sqrt{2}}{m_\rho}\langle {}^3P_1|rf_\rho(r)|{}^3D^{(-)}_1\rangle_d\Bigg], \end{aligned} \tag{A14}$$

$$\begin{aligned} X_4 = -\frac{4\sqrt{2}}{\sqrt{3}(m^2_\rho - m^2_\pi)}\Bigg(&\langle {}^3P_1|f'_{\pi\rho}(r)|{}^3S_1\rangle_d \\ &+ \frac{1}{\sqrt{2}}\langle {}^3P_1|f'_{\pi\rho}(r)|{}^3D_1\rangle_d\Bigg); \end{aligned} \tag{A15}$$

(3) $^3P_2$–$^3F_2$

$$X_1 = \frac{\sqrt{5}}{3}\left[\langle {}^3P_2|rf_\rho(r)|{}^3S_1\rangle_d - \frac{2\sqrt{2}}{5}\langle {}^3P_2|rf_\rho(r)|{}^3D_1\rangle_d - \frac{3\sqrt{3}}{5}\langle {}^3F_2|rf_\rho(r)|{}^3D_1\rangle_d\right], \tag{A16}$$

$$X_2 = -\frac{\sqrt{5}}{3}\left(\langle {}^3P_2|rf_\omega(r)|{}^3S_1\rangle_d - \frac{2\sqrt{2}}{5}\langle {}^3P_2|rf_\omega(r)|{}^3D_1\rangle_d - \frac{3\sqrt{3}}{5}\langle {}^3F_2|rf_\omega(r)|{}^3D_1\rangle_d\right), \tag{A17}$$

$$X_3 = \frac{4\sqrt{5}}{3}\left((1-\mu_v)\langle {}^3P_2|rf_\rho(r)|{}^3S_1\rangle_d - \frac{2\sqrt{2}}{5}(1-4\mu_v)\langle {}^3P_2|rf_\rho(r)|{}^3D_1\rangle_d - \frac{2}{m_\rho}\langle {}^3P_2|rf_\rho(r)|{}^3S_1^{(+)}\rangle_d + \frac{4\sqrt{2}}{5m_\rho}\langle {}^3P_2|rf_\rho(r)|{}^3D_1^{(-)}\rangle_d \right.$$
$$\left. - \frac{3\sqrt{3}}{5}(1+\mu_v)\langle {}^3F_2|rf_\rho(r)|{}^3D_1\rangle_d + \frac{6\sqrt{3}}{5m_\rho}\langle {}^3F_2|rf_\rho(r)|{}^3D_1^{(+)}\rangle_d\right), \tag{A18}$$

$$X_4 = \frac{4\sqrt{10}}{3(m_\rho^2 - m_\pi^2)}\left(\langle {}^3P_2|f'_{\pi\rho}(r)|{}^3S_1\rangle_d - \frac{1}{5\sqrt{2}}\langle {}^3P_2|f'_{\pi\rho}(r)|{}^3D_1\rangle_d + \frac{3\sqrt{3}}{5}\langle {}^3F_2|f'_{\pi\rho}(r)|{}^3D_1\rangle_d\right), \tag{A19}$$

where

$$|{}^{2S+1}L_J^{(+)}\rangle \equiv \left(\frac{d}{dr} - \frac{L+1}{r}\right)|{}^{2S+1}L_J\rangle,$$

$$|{}^{2S+1}L_J^{(-)}\rangle \equiv \left(\frac{d}{dr} + \frac{L}{r}\right)|{}^{2S+1}L_J\rangle,$$

and

$$f'_{\pi\rho}(r) \equiv \frac{d}{dr}[f_\pi(r) - f_\rho(r)].$$

[1] G. S. Danilov, Phys. Lett. **18**, 40 (1965).
[2] V. M. Lobashov *et al.*, Nucl. Phys. **A197**, 241 (1972).
[3] K. R. Lassey and B. H. J. McKellar, Phys. Rev. C **11**, 349 (1975).
[4] B. Desplanques, Nucl. Phys. **A242**, 423 (1975).
[5] B. A. Craver, E. Fischbach, Y. E. Kim, and A. Tubis, Phys. Rev. D **13**, 1376 (1976).
[6] V. A. Knyazkov *et al.*, JETP Lett. **38**, 163 (1983).
[7] V. A. Knyazkov *et al.*, Nucl. Phys. **A417**, 209 (1984).
[8] A. R. Berdoz *et al.*, Phys. Rev. Lett. **87**, 272301 (2001).
[9] W. M. Snow *et al.*, Nucl. Instrum. Methods Phys. Res. A **440**, 729 (2000).
[10] R. Hasty *et al.*, Science **290**, 2117 (2000).
[11] T. M. Ito *et al.*, Phys. Rev. Lett. **92**, 102003 (2004).
[12] H. C. Lee, Phys. Rev. Lett. **41**, 843 (1978).
[13] T. Oka, Phys. Rev. D **27**, 523 (1983).
[14] I. B. Khriplovich and R. V. Korkin, Nucl. Phys. **A690**, 610 (2001).
[15] E. D. Earle, A. B. McDonald, and J. W. Knowles, *An experiment to measure parity violation in the $^2H(\gamma,n)H$ reaction*, AIP Conf. Proc. No. 69, (AIP, New York, 1981), p. 1436.
[16] E. D. Earle *et al.*, Can. J. Phys. **66**, 534 (1988).
[17] B. Wojtsekhowski and W. T. H. van Oers, JLab letter-of-intent 00-002.
[18] A. J. F. Siegert, Phys. Rev. **52**, 787 (1937).
[19] B. Desplanques, J. F. Donoghue, and B. R. Holstein, Ann. Phys. (N.Y.) **124**, 449 (1980).
[20] M. J. Musolf *et al.*, Phys. Rep. **239**, 1 (1994).
[21] C.-P. Liu, G. Prézeau, and M. J. Ramsey-Musolf, Phys. Rev. C **67**, 035501 (2003).
[22] C.-P. Liu, C. H. Hyun, and B. Desplanques, Phys. Rev. C **68**, 045501 (2003).
[23] R. B. Wiringa, V. G. J. Stoks, and R. Schiavilla, Phys. Rev. C **51**, 38 (1995).
[24] H. Arenhövel and H. Sanzone, Few-Body Syst., Suppl. **3**, 1 (1991).
[25] J. Missimer, Phys. Rev. C **14**, 347 (1976).
[26] B. Desplanques and J. Missimer, Nucl. Phys. **A300**, 286 (1978).
[27] B. R. Holstein, URL: http://mocha.phys.washington.edu/~int_talk/WorkShops/int_02_3/People/Holstein_B/
[28] B. Desplanques, Phys. Rep. **297**, 1 (1998).
[29] R. Schiavilla, URL: http://mocha.phys.washington.edu/~int_talk/WorkShops/int_03_3/People/Schiavilla_R/
[30] J. L. Friar and B. H. J. McKellar, Phys. Lett. **123B**, 284 (1983).
[31] E. Truhlik, J. Smejkal, and F. C. Khanna, Nucl. Phys. **A680**, 741 (2001).